Journal of Engineering Sciences
Vol 10, Issue 11, Nov /2019
ISSN NO:0377-9254

MULTI-FOCUS IMAGE FUSION ALGORITHM IN SENSOR NETWORKS

L.PALLAVI [1], T.MAHABOOB RASOOL [2]
[1]PG Student, Dept of DECS, BCETFW, Kadapa, AP ,India.
[2]Assistant Professor, Dept of DECS, BCETFW, Kadapa, AP ,India.

ABSTRACT- Most imaging systems have a limited depth-of-field in the sensor networks that consist of multiple visual sensors. Due to different object distances, not every object can be clearly imaged by a single sensor. This paper proposes a multi-focus image fusion algorithm in sensor networks. The algorithm combines the advantages of multi-scale analysis and image phase analysis. It uses dynamic window and phase stretch transform (PST) to extract the focused regions of each image accurately and performs multi-resolution analysis of images through the non-sub-sampled shearlet transform. Then, the images are fused according to the local standard deviation of PST feature maps. The results of the simulation experiments prove that our algorithm is effective and outperforms some state-of-the-art algorithms.

I. INTRODUCTION

Now a day's numerous criteria that define the characteristics of a high quality image such as sharp, focus, be properly exposed, having correct color balance, and not having too much noise have been proposed and discussed extensively in image processing literature. Image quality has as much to do with user applications and requirements as it does with perceived visual quality in general. There are many techniques to get a good image or a high quality image. One of them is image fusion technique. Image fusion is an important research topic in many related areas such as computer vision, automatic object detection, remote sensing, image processing, robotics, and medical imaging. The need for image fusion in current image processing systems is increasing mainly due to the increased number and variety of image acquisition techniques. Multi-focus image fusion is the process of combining relevant information from several images into one image.

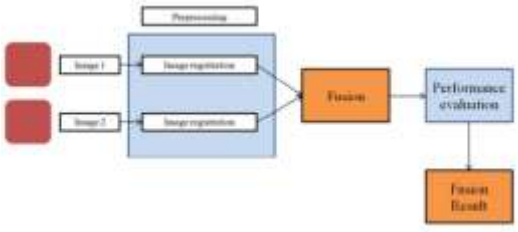

Fig.1. Image fusion process

Sensor networks play an important role in the new generation of information technology. It can collect plenty of information that needs to be connected, supervised or interacted in real time through various sensing devices, and combine them with the Internet to form a huge network. Sensor networks can realize the connection between objects, people and networks, so as to facilitate object identification, information management and control. In the perception layer of sensor networks, information acquisition is mainly realized by different kinds of sensing devices, among which vision sensors have been widely used. The main subject of vision sensor application is machine vision, which is commonly applied to object recognition, 3D positioning, target tracking, industrial measurement and so on. Most of the applications of machine vision are based on a clear and all-in-focus image. Because every image sensor has a limited depth-of-field, only the objects within a certain distance can be clearly imaged. The objects which are closer or farther than that often appear out-of-focus. In order to obtain a clear all-in-focus image, different objects in the scene need to be focused separately by different image sensors, and then be fused together by an image processing method. Therefore, the multi-focus image fusion technology has gradually become an important research content in the networks of vision sensors. Multi-focus image fusion is an important branch in the field of multi-source image fusion. It needs to register multiple images of the same scene, then use some method to extract the clear regions of each image, and integrate them into an all-in-focus image. Therefore, one of the difficulties is to judge the focused regions from different images accurately. Multi-focus image fusion can be carried out on three different levels: pixel level, feature level and decision level. Pixel level image fusion is the foundation of the others. It is a hot issue in the field of image fusion, and it is also the topic of this project. The advantage of pixel level image fusion is that it can keep the original information of the source image as much as possible and obtain rich and accurate image details. The fusion accuracy of pixel level image fusion is the highest among the three. However, its processing time is longer and it also requires higher registration accuracy. At present, the algorithms used in pixel level multi-focus image fusion mainly include: principal component analysis, support vector machine, neural network, image segmentation, multi-scale analysis and so on, and many new algorithms are also emerging in an

endless stream. Bai *et al.* proposed a multi-focus image fusion algorithm through gradient-based decision map construction and mathematical morphology. Yang *et al.* present a novel multi-focus image fusion framework based on non-subsampled contourlet transform and sparse representation. Yang *et al.* proposed a fusion scheme based on block-matching and 3D multi-scale transform. In this project, a multi-focus image fusion algorithm based on Non-subsampled Shearlet Transform (NSST) multi-scale analysis and Phase Stretch Transform (PST) feature extraction is proposed. NSST is a new multi-resolution analysis transform developed in recent years. It has been widely used in the field of image processing. In our previous study, NSST has been successfully applied to compressive image fusion and image enhancement. Most existing transform domain image fusion algorithms pay much attention to the amplitude of image decomposition coefficients. However, the phase information of image also plays a very important role in image interpretation and recognition. Image phase information analysis has been widely used in image registration, mosaic and other fields. In this paper, the image phase information is used as the reference for extracting features of images. The focused regions of the source images are accurately judged by the Local Standard Deviation (LSD) of PST feature maps, and then the coefficients of each scale are fused accordingly. Experiments show that the extraction of the focused regions is accurate and effective.

II. EXISTING SYSTEM

Bandelet transform has undergone two generations of transform theory, and its main application fields are image sparse expression and image compression. Among them, Pennec for the first generation of Bandelet transform made an important contribution, he not only involved in the proposed first generation Bandelet transform theory, but also further on the Bandelet transform to improve and develop, greatly enhance its practical application. The biggest advantage of Bandelet transform is that it makes up the defects of wavelet transform anisotropic feature, which is more favorable for sparse expression and sparse coding of image. The first generation Bandelet transform technique is based on the theory of wavelet transform, from reasoning to evolution and evolution of continuous, and then relying on the concept of geometric flow to construct Bandelet transform basis function, so as to promote discrete Bandelet transform algorithm, continuous bandlet transform algorithm. First, the Bandelet transform defines a geometric vector line to characterize the local regular direction of the image. The binary section method is used to subdivide the support interval S of the image.

$$S = \cup \ \Omega i.$$

Time, each of the small split interval Q contains only a certain contour in the image. However, the gray scale variation in the region Q that does not contain any contour lines is uniform and does not need to define any geometric vector lines in these local regions. The geometric regular direction in the local region Q containing a contour is The tangent direction of the contour line, which contains the sub-region of the contour line, is marked as horizontal and vertical. Under the global optimal constraint, the local vector flow on the vector field τ (x1, x2) on the local region Ωi can be calculated according to the obtained local geometric regular direction. Then, Bandlet can be processed by the interval wavelet with the Ban-delet blocks along the vector flow to generate the required Bandelet base. Through this process, we can make full use of the local geometric regularity of the image itself, and the set of Bandelet bases on all the subdivided regions constitute a set of standard orthogonal bases on L2 (S). In the geometric direction, assuming that the image equation is regular, for this geometric regular image, the image changes in the direction parallel to the edge line, and changes in the direction perpendicular to the edge line. The geometric flow in the image generally refers to the vector field τ (x1, x2) defined on the support area of the image, which is used to describe the direction of the regular change of each point. For parallel to the edge of the line direction, you can use geometric flow to describe.

The primary purpose of the Bandelet transform is to make full use of the regularity of the image along the geometric flow. Near the edge line, the geometric flow is generally parallel to the tangent direction of the edge line, and for geometric regular images, the geometric flow in the local range is generally parallel. In order to reduce the data overhead and simplify the algorithm, the bandlet transform algorithm is used to merge the adjacent subbands with similar geometric flow characteristics in the pre-segmentation. After the optimization of the quadtree, the basic Represents the result of image processing. Let the bottom of the small box width of 4 pixels, that is, the size of 4 * 4. Bandelet process is the two-dimensional wavelet coefficients stored in the Bandelet block, resampling along the best geometric flow direction θ, generating one-dimensional data, and transforming the one-dimensional data using one-dimensional Wavelet transform. The one-dimensional wavelet transform is carried out in the direction of the optimal geometric flow to find the discontinuous direction, and then the wavelet transform is carried out along these directions. In addition, a method of projecting two-dimensional

information into one-dimensional information along the optimal geometric direction can be used to convert the two-dimensional singularity into point singularity. The basic flow of the algorithm is: 1) input the image that needs to be processed; 2) set the quantization threshold T according to the experience; 3) make the wavelet transform of the input image by biorthogonal wavelet transform; 4) And then calculating the optimal geometric flow direction in each segmented region. 5) For each bandletlet block, that is, the Bandelet subband, the Bandelet processing is performed separately, and the corresponding sub-band is divided into two sub- 6) the resulting Bandelet coefficients are arranged in the form of the corresponding matrix according to the basic principles and methods of the Bandelet transform; 7) the resulting quadtree structure, the best geometric flow direction and the Ban-delet directions. The *bandelet* is designed to use the geometric flow direction to find the optimal representation of linear structures when an image is decomposed, which gives an advantage over other methods because geometric structures carry most of the perceptual information in the image. Geometric structures can be easily represented along a set of curves that have singularity in an image. Difficulty arises in the fact that most images do not contain this simplistic singularity, but instead possess textural content that has relevance in both its noise and its curves.

Bandelets have been used in conjunction with contourlets to denoise images, detect edges in text, fuse images, cluster features, construct sparse image representation, and perform surface compression. Bandelets are one of the multiresolution transforms constructed to handle the directional shortcomings of the wavelet transform. The bandelet computes a geometric flow of an image in order to better capture smooth edge information. A bandelet decomposition is applied to the orthogonal wavelet coefficients, or wavelet filter bank, of an image and is computed with a geometric orthogonal transform via directional orthogonal filters. A different transform will result from each geometric direction and these can be processed to find the optimal set of filters with a best basis algorithm. One can manipulate the characteristics of the wavelets through a choice of low pass and high pass quadrature mirror filters. By selecting a decomposition such that the scale of the resulting sub-bands and zoom in on a singularity in the transform to a sub-square *S*, the wavelet coefficients are samples of the regularized function that underlies the bandelet decomposition that follows:

$$\langle f, \psi_{jn} \rangle = f * \psi_j(2^j n)$$

Here we note that

$$\psi_j(x) = \frac{1}{2^j}\psi(-2^{-j}x)$$

the wavelet coefficients are sections of a regularized function that are derived from the convolution of the original function with a blur kernel, despite the possibility of the primordial function being singular along the edges. Since one does not know the equations of the curves a priori, it is obligatory to estimate the geometry using discrete image information, in practice. To manage geometrical estimation, the bandelet process involves discovering flow direction along the most regular direction and searching for a polynomial flow of degree *p*-1 that is parameterized. Just one of either the vertical or horizontal parameters is sufficient. Following directional analysis, an optimal polynomial flow is defined on an optimal sub-square, *S*. It can be
shown that given that an integral curve of geometric flow does not deviate more than one pixel in wavelet space from the real geometry that the explicit bound of the derivatives of *f* in the direction of the flow and in the vertical direction is

$$\left|\frac{\partial^{a+b} f}{\partial \tau^a \partial y^b}\right| \leq C 2^j 2^{(-a/\propto j)} 2^{-jb}$$

where *a* and *b* are constant parameters used to drive the polynomial approximation for towards the elongated flow in the small bands of the construction are real valued constants. The direction that is orthogonal to is denoted as *y*. An orthogonal filter bank is formulated to decompose for functions that follow the geometric flow. This will allow for the approximation of the function on the regular grid of spacing in the localized region *S* once the approximate geometric flow has been obtained. The support for the filters is derived using dyadic grouping of the sampling points in the local region into bands expressed as for each step *k* in the filtering process. The filters are calculated using a transform procedure that implements Gram-Schmidt orthogonalization. These will have *p* vanishing moments, tantamount to the original wavelet basis; however, they are elongated along the singularity in disparity with the square support of a wavelet. To apply the aforementioned modus operandi across the entire image domain, it is imperative to have an effective method of creating the sub-squares that partition the domain. Quadtree segmentation of each wavelet scale in dyadic squares is utilized for image partition. A different quadtree will be used for each scale of the wavelet transform, but the same quadtree is used on each of the subbands at each decomposition level. A complete bandelet basis, denoted is composed of an image segmentation at each scale defined by a quadtree, and a polynomial flow and bandelet coefficients for each dyadic square in the quadtree segmentation at each level.

In the bandelet-based fusion algorithm, bandelet transform is used as a MSD tool for images. It can extract the features of original

images well, such as edges and texture, so that more information is provided for fusion. The fusion framework using bandelet transform is shown in Fig.2. The operational procedure for the proposed bandelet-based image fusion approach is given as follows.

1) The two source images in the fusion are geometrically registered to each other.

2) Compute the image sample values along the flow lines in each region Ωi of the partition.

3) Geometric flow Gj (i) $(j = 1, 2, \cdots, N)$ in each region Ωi and bandelet coefficients Cj (x, y, i) $(j = 1, 2, \cdots, N)$ corresponding to the geometric flow are computed. N is the total number of source images, Cj (x, y, i) is the bandelet coefficient of jth source image at the pixel (x, y) and $(x, y) \in \Omega i$.

4) Process the fusion rules. For the geometric flow, fusion with the maximum rule

$$G_{\mathrm{F}}(i) = \begin{cases} G_1(i), & \text{if } G_1(i) \geq G_2(\\ G_2(i), & \text{if } G_1(i) < G_2(\end{cases}$$

For the bandelet coefficients, fusion with the maximum absolute value rule:

$$C_{\mathrm{F}}(x,y,i) = \begin{cases} C_1(x,y,i), & \text{if } \mathrm{abs}(C \\ & \geq \mathrm{abs}(C \\ C_2(x,y,i), & \text{if } \mathrm{abs}(C \\ & < \mathrm{abs}(C \end{cases}$$

The GF (i) denotes the geometric flow in the region Ωi of the fused image, CF (x, y, i) is the bandelet coefficient of fused image at the pixel (x, y) and $(x, y) \in \Omega i$.

5) The fused image is reconstructed by the bandelet inverse transform using geometric flow GF (i) and bandelet coefficients CF (x, y, i).

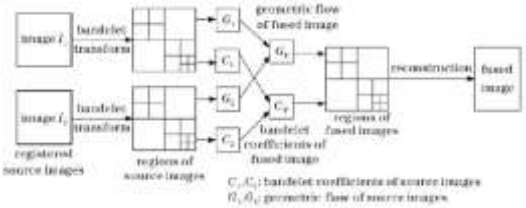

Fig.2. Fusion framework using bandelet transform.

The performance evaluation criteria of image fusion are still a hot topic in the research of image fusion. Besides visual observation, objective performance evaluation criteria are used in this paper, such as the standard deviation, average gradient, entropy, and mutual information. To evaluate the performance of the proposed fusion algorithm, we compare in with two typical algorithms: the maximum algorithm based on wavelet transform and the maximum algorithm based on Laplacian pyramid.

Fig.3. Source images in the fusion experiment.

In the experiment, two blurred images are used as source images, as shown in Fig.3. The source images are 256 × 256 in size and 256 levels in gray value. It can be seen that Fig. 3(a) is clear in circumjacent region around the center of the image and blurred in the center region. In contrast, Fig. 3(b) is clear in the center region and blurred in circumjacent region. Our aim is to obtain a totally clear image.

III. PROPOSED SYSTEM

In this project, a multi-focus image fusion algorithm based on Non-subsampled Shearlet Transform (NSST) multi-scale analysis and Phase Stretch Transform (PST) feature extraction is proposed. NSST is a new multi-resolution analysis transform developed in recent years. It has been widely used in the field of image processing. In our previous study, NSST has been successfully applied to compressive image fusion and image enhancement. Most existing transform domain image fusion algorithms pay much attention to the amplitude of image decomposition coefficients. However, the phase information of image also plays a very important role in image interpretation and recognition. Image phase information analysis has been widely used in image registration, mosaic and other fields. In this paper, the image phase information is used as the reference for extracting features of images. The focused regions of the source images are accurately judged by the Local Standard Deviation (LSD) of PST feature maps, and then the coefficients of each scale are fused accordingly.

A. NSST MULTISCALE ANALYSIS

NSST is a new multi-scale and multi-directional analysis tool. The NSST decomposition procedure is shown briefly in Fig. 4. According to the principle of NSST, the source image will be decomposed into low frequency coefficients and high frequency coefficients after Non-down-sampling Pyramid Decomposition (NSP), and then NSP decomposition of each layer will iterate on the low frequency component of the former layer. The band-pass images and a low pass image can be obtained after decomposition. Since there is no

down-sampling in the NSST process, these images are of the same size as the original image.

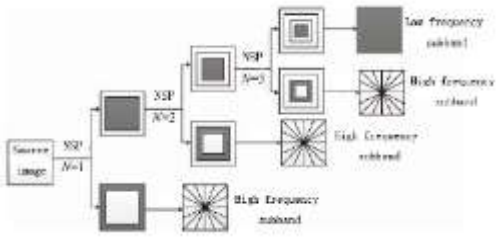

Fig.4. NSST decomposition procedure.

B. FEATURE EXTRACTION WITH PST

PST is a new signal transform proposed in these years. It performs well in image feature extraction, especially edge extraction. The process of PST feature extraction includes multiple steps: First of all, smooth the image with low-pass filtering so as to remove noise. Furthermore, let the image pass through a non-linear frequency dependent transfer function which is called PST kernel. The output of the transform is the phase in space domain. The applied phase is frequency dependent with the original image, that is higher amount of phase is applied to higher frequency component. Finally, find image sharp transitions by thresholding the phase and apply binary morphological post-processing, so as to enhance the features and clear the transformed image. PST is defined as (1) in frequency domain.

$$A[n,m] = \angle\{IFFT2\{\tilde{K}[p,q] \cdot \tilde{L}[p,q] \cdot FFT2\{B[n,m]\}\}\} \quad (1)$$

where n and m are the two dimensional space domain variables, $A[n,m]$ is the output phase feature map, $B[n,m]$ is the input image, FFT2 is the 2-D Fast Fourier Transform, IFFT2 is the inverse operation of FFT2. p and q are the two dimensional frequency domain variables. The function KQ $[p; q]$ is the phase kernel and LQ $[p; q]$ is the frequency response of the localization kernel.

C. IMAGE FUSION SCHEME

The image fusion method proposed in this paper is based on the multi-scale decomposition of NSST. PST is applied to extract the details of each original image. Then we form different size of windows on the PST feature map for different scales of coefficients in order to justify the clarity of the local area, so the focused region of each image can be extracted gradually. After that, the coefficients are fused based on the fusion rule in focused area, transition area, and out-of-focus area. And finally the inverse NSST are used to reconstruct the final fused image.

1) FEATURE EXTRACTION

Texture is a kind of typical image feature. In the focused regions of images, texture is usually clear and intact. Therefore, our algorithm takes the extraction of image texture feature as an important step of judging the focused areas of multi-focus images. PST algorithm has obvious advantages in image edge and texture extraction. It has been proved that PST can extract image features accurately at low contrast or visually impaired images. In this paper, PST is used to extract the features of original images. The output image with texture features is called PST feature map. Fig. 5 is the result of PST feature extraction of multi-focus images. Fig. 5(a) and Fig.5 (b) are the original images of Pepsi image set. Fig.5 (c) is the feature map of Fig.5 (a), while Fig.5 (d) is the feature map of Fig.5(b). We can see that the textures of the focused area are clear and rich, in comparison, the textures of the defocused area are fuzzy and blurry. Therefore, the change of the local area contrast of the feature map can be considered as the reference for judging the focused areas.

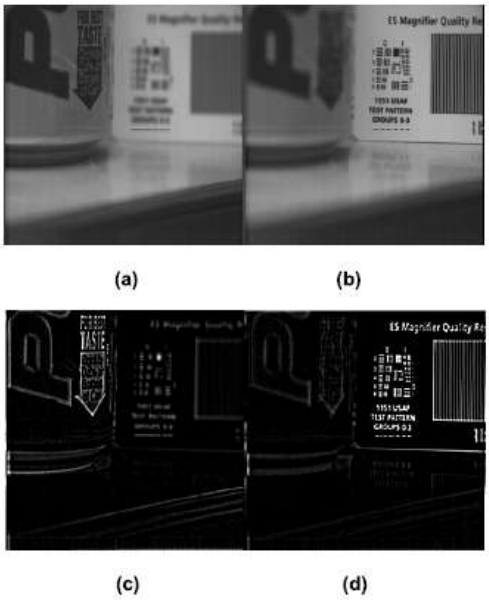

Fig.5. PST feature map (a) Pepsi1 (b)Pepsi2 (c) PST feature map of Pepsi1 (d) PST feature map of Pepsi2.

2) EXTRACTION OF THE IMAGE FOCUSED REGIONS

The PST feature map contains the texture information of the original image. It can be seen from Fig.5 that the focused areas and the out-of-focus regions of the original images can be roughly judged by subjective observation of human eyes. The main basis of our judgment is the contrast change of the feature map. The part where the contrast changes brightly in the feature map always corresponds to the focused area of the original image, whereas the part where the contrast change is gentle often corresponds to the blurred area. For machine vision, there are many ways to judge the contrast change. Among them, the most commonly used and effective method is to calculate the LSD

of the image. The LSD reflects the contrast variation in an image by a local window centered at the current pixel. The gray value of the image has a large fluctuation in the place where the LSD is large; on the other hand, if the LSD is small, the change of the gray scale of the image will be slow and gentle. In this paper, a local window is sliding on the PST feature map to calculate the standard deviation in the local area of each pixel, and the focused area of the image is judged according to the value of LSD. However, the value depends not only on the features of the image itself, but also on the size of the local window. Commonly, the window size is set to be (2*n* C 1) _ (2*n* C 1), where *n* is an integer. The larger the *n* values, the more pixels will be used to calculate the LSD, and the longer the process will take; the smaller the *n* values, the shorter the process will take, but the LSD only reflects the change of gray scale in a small range. This algorithm uses NSST to decompose the image into different scales, and the image coefficients of various scales have different features. Fig. 6 shows the coefficients of each layer after NSST three-scale-decomposition (each layer is decomposed into 8 directions) of image Pepsi. By contrast, it is found that with the increase of decomposition scale, the image information embodied in each layer's components is gradually refined. Therefore, the window size for calculating LSD should also be adjusted accordingly.

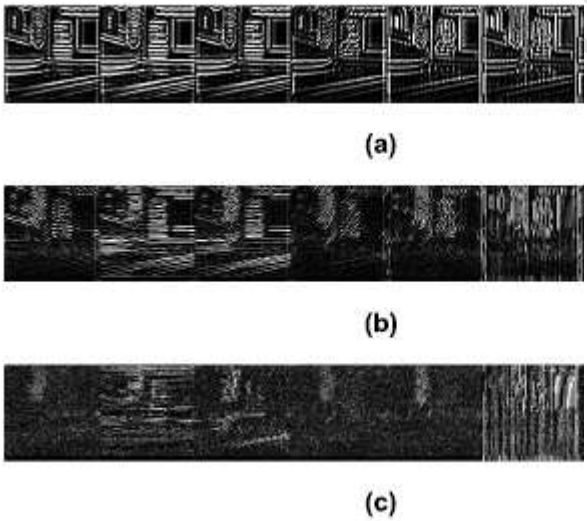

Fig.6. Sub-band components images of NSST (a) The components of the first layer (b) The components of the second layer (c) The components of the third layer.

In order to select the appropriate window size to calculate LSD for each scale, a focused area extraction experiment was proposed. The main steps are as follows:

(1) Divide a rectangle region from image Lena artificially, as shown in Fig.7. Then add defocus blur in the area around the graph, as is shown in Fig.7(a). In Fig.7(b), add defocus blur in the rectangle region in the middle of Lena.

(2) Decompose the two images into three scales by NSST, and get the PST feature map of each image separately, as shown in Fig.8.

Fig.7. Lena Image set with artificial defocus blur (a) Lena with defocus blur in the surrounding area (b) Lena with defocus blur in the middle area.

Fig.8. PST feature maps of Fig.7 (a) PST feature map of Fig.7(a) (b) PST feature map of Fig.7(b).

(3) The NSST image coefficients are compared layer by layer according to the order of low scale to high scale so as to extract the focused areas. The comparison is based on the LSD of the PST feature map, as shown in (2).

$$\begin{aligned} &if\ LSD_{N_l}1(i,j) >= LSD_{N_l}2(i,j)\ then \\ &\quad I^{l,d}(i,j) = 0 \\ &else \\ &\quad I^{l,d}(i,j) = 255 \end{aligned}$$

where *Nl* indicates the size of the local window for layer *l* that used to calculate the LSD of PST feature map. *LSDNl* 1(*i*; *j*) represents the value of the LSD in the PST feature map at the location of (*i*,*j*) of the first image, while *LSDNl* 2(*i*; *j*) represents the value of the LSD in the PST feature map of the second image. *I l*;*d* (*i*; *j*) represents the value of the NSST coefficient of the focused region extraction graph *I* at direction *d* layer *l*.

(4) NSST inverse transform is performed on *I l*;*d* (*i*; *j*), and the final focused region extraction graph *I* is formed.

Fig.9 is the focused region extraction graphs calculated by different size of local window.

Vol 10, Issue 11, Nov /2019
ISSN NO:0377-9254

The black parts in each graph represent the focused areas of Fig. (a), and the white parts indicate the focused areas of Fig. (b). *N1* is the size of the local window for the first layer; *N2* is the size of the local window for the second layer, while *N3* represents the size of the local window for the third layer.

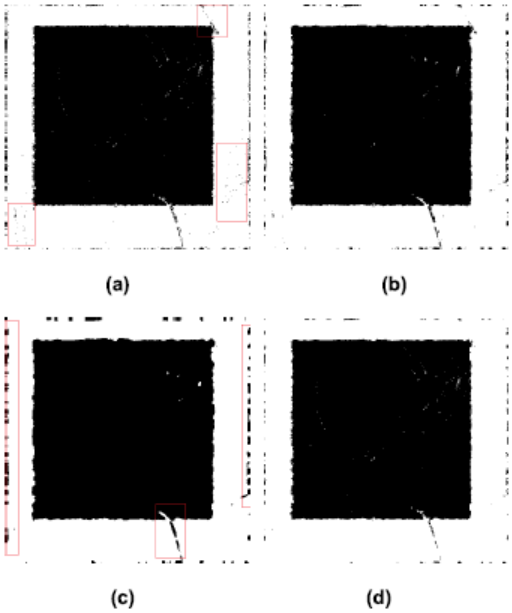

Fig.9. Extraction effects of focused areas in Lena image set (a) N1D3,N2D3,N3D3 (b) N1D5,N2D5,N3D5 (c) N1D9,N2D9,N3D9 (d) N1D9,N2D5,N3D3.

Through comparison of the above graphs, it can be seen that when the sizes of the local windows are different, the extraction effects of the focused regions are various (as shown in the red boxes in the pictures), especially for the focus transition regions and the edges of the images. From Fig. (a) to Fig. (c), the local window size increases gradually. The number of isolated and scattered mis-extraction pixels reduces obviously, but meanwhile the errors at the edges of images and the transition regions are more serious. Fig. (d) uses different local window size for different layer, which makes a good compromise between the two trends, and the focused areas extraction is more complete and accurate. So in our algorithm, the local window used to calculate the LSD of PST feature map is variable-sized, that is smaller size corresponds to higher frequency components.

3) IMAGE FUSION RULE

The image fusion rule of our algorithm is based on the extraction of the focused regions. The NSST decomposition coefficients of each layer are fused according to the fusion rule, and the fused image is composed by the NSST inverse transform. The image fusion rule is shown as (3):

$$
\begin{aligned}
&\text{if } LSD_{N_l}1(i,j) > LSD_{N_l}2(i,j)\\
&\quad F^{l,d}(i,j) = \mathrm{I1}^{l,d}(i,j)\\
&\text{else if } LSD_{N_l}1(i,j) = LSD_{N_l}2(i,j)\\
&\quad F^{l,d}(i,j) = (\mathrm{I1}^{l,d}(i,j) + \mathrm{I2}^{l,d}(i,j))/2\\
&\text{else}\\
&\quad F^{l,d}(i,j) = \mathrm{I2}^{l,d}(i,j)
\end{aligned}
$$

where $Fl;d\ (i;\ j)$ represents the NSST coefficient at direction d layer l of the fused image. $I1l;d\ (i;\ j)$ is the NSST coefficient of the first image, while $I2l;d\ (i;\ j)$ is the NSST coefficient of the second image. This algorithm follows the fusion rule of taking the maximun LSD of the PST feature map. When the LSDs of the PST feature maps of the source images are equal, the coefficient of the fused image is set to be the mean value of the coefficients of the source images.

IV. RESULTS

input1

input2

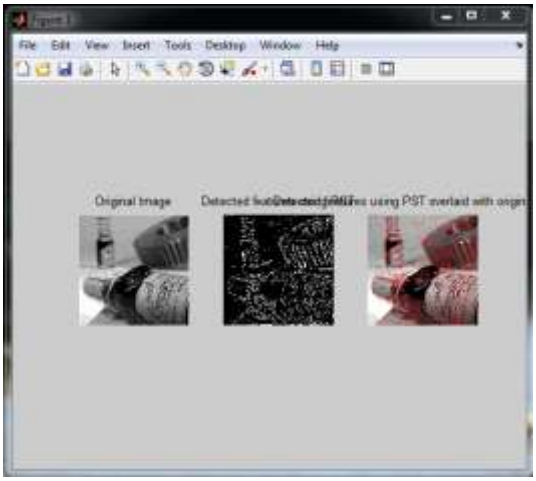

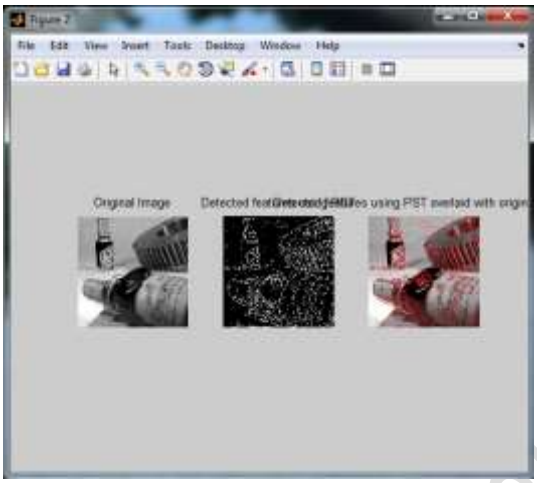

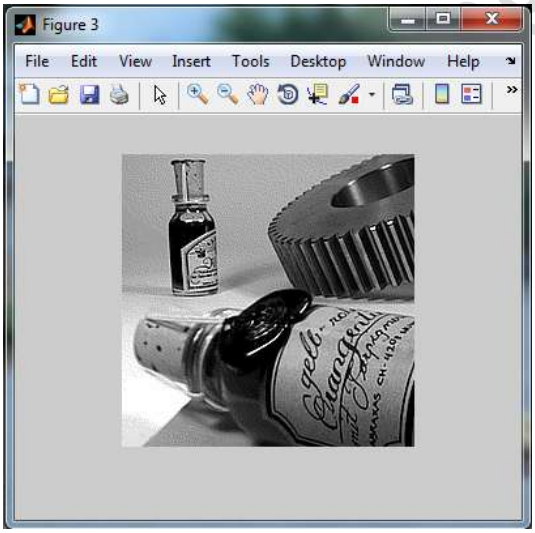

V. CONCLUSION

In this project, a multi-focus image fusion algorithm is proposed, which is used to synthesize images from multiple visual sensors into a fully focused image in sensor networks. PST feature map is used as the reference to determine the focused regions. Then decompose the images by NSST and fuse them according to the LSD of the PST feature maps. Experiments show that our algorithm can extract the focused areas of different source images exactly and fused them without introducing any artifacts. The boundaries between the focused regions are smooth and natural. The contrast of the original images can be well preserved.

REFERENCES

[1] F. Zhao, L.Wei, and H. Chen, ``Optimal time allocation for wireless information and power transfer in wireless powered communication systems," *IEEE Trans. Veh. Technol.*, vol. 65, no. 3, pp. 1830_1835, Mar. 2016.
[2] F. Zhao, H. Nie, and H. Chen, ``Group buying spectrum auction algorithm for fractional frequency reuse cognitive cellular systems," *Ad Hoc Netw.*, vol. 58, pp. 239_246, Apr. 2017.
[3] F. Zhao, B. Li, H. Chen, and X. Lv, ``Joint beamforming and power allocation for cognitive MIMO systems under imperfect CSI based on game theory," *Wireless Pers. Commun.*, vol. 73, no. 3, pp. 679_694, 2013.
[4] F. Zhao, W. Wang, H. Chen, and Q. Zhang, ``Interference alignment and game-theoretic power allocation in MIMO Heterogeneous Sensor Networks communications," *Signal Process.*, vol. 126, pp. 173_179, Sep. 2016.
[5] Y. Yang *et al.*, ``Multi-focus image fusion via clustering PCA based joint dictionary learning," *IEEE Access*, vol. 5, pp. 16985_16997, Aug. 2017.
[6] Q. Jiang, X. Jin, S.-J. Lee, and S. Yao, ``A novel multi-focus image fusion method based on stationary wavelet transform and local features of fuzzy sets," *IEEE Access*, vol. 5, pp. 20286_20302, Oct. 2017.
[7] C. Du and S. Gao, ``Image segmentation-based multi-focus image fusion through multi-scale convolutional neural network," *IEEE Access*, vol. 5, pp. 15750_15761, Aug. 2017.
[8] X. Bai, M. Liu, Z. Chen, P.Wang, andY. Zhang, ``Multi-focus image fusion through gradient- based decision map construction and mathematical morphology," *IEEE Access*, vol. 4, pp. 4749_4760, Aug. 2016.
[9] Y. Dongsheng, H. Shaohai, L. Shuaiqi, M. Xiaole, and S. Yuchao, ``Multi- focus image fusion based on block matching in 3D transform domain," *J. Syst. Eng. Electron.*, vol. 29, no. 2, pp. 415_428, Apr. 2018.
[10] Y. Tong and J. Chen, ``Non-linear adaptive image enhancement in wireless sensor networks based on non-subsampled shearlet transform," *EURASIP J. Wireless Commun. Netw.*, vol. 2017, no. 1, p. 46, 2017.
[11] Y. Tong and J. Chen, ``Compressive sensing image fusion in heterogeneous sensor networks based on shearlet and wavelet transform," *EURASIP J. Wireless Commun. Netw.*, vol. 2017, no. 1, p. 52, 2017.

[12] M. Suthar, H. Asghari, and B. Jalali, ``Feature enhancement in visually impaired images," *IEEE Access*, vol. 6, pp. 1407_1415, Dec. 2017.
[13] M. H. Asghari and B. Jalali, ``Edge detection in digital images using dispersive phase stretch transform," *Int. J. Biomed. Imag.*, vol. 2015, Jan. 2015, Art. no. 687819.
[14] X. Qu, J. Yan, G. Xie, Z. Zhu, and B. Chen, ``A novel image fusion algorithm based on bandelet transform," *Chin. Opt. Lett.*, vol. 5, no. 10, pp. 569_572, 2007.
[15] K. Zhan, J. Teng, Q. Li, and J. Shi, ``A novel explicit multi-focus image fusion method," *J. Inf. Hiding Multimedia Signal Process.*, vol. 6, no. 3, pp. 600_612, 2015.
[16] S. Paul, I. S. Sevcenco, and P. Agathoklis, ``Multi-exposure and Multifocus Image Fusion in Gradient Domain," *J. Circuits Syst. Comput.*, vol. 25, no. 10, 2016, Art. no. 1650123.
[17] Z. Liu, E. Blasch, Z. Xue, J. Zhao, R. Laganiere, and W. Wu, ``Objective assessment of multiresolution image fusion algorithms for context enhancement in night vision: A comparative study," *IEEE Trans. Pattern Anal. Mach. Intell.*, vol. 34, no. 1, pp. 94_109, Jan. 2012.
[18] M. S. Farid, A. Mahmood, and S. A. Al-Maadeed, ``Multi-focus image fusion using content adaptive blurring," *Inf. Fusion*, no. 45, pp. 96_112, Jan. 2018.